CHEMISTRY OF MATERIALS
Article

Chem. Mater. **2010,** *22,* 1695–1703 1695
DOI:10.1021/cm9031072

Mesoporous Microcapsules with Decorated Inner Surface: Fabrication and Photocatalytic Activity

Yuri Yamada,* Mamoru Mizutani, Tadashi Nakamura, and Kazuhisa Yano

Toyota Central Research & Development Laboratories, Inc., Nagakute, Aichi 480-1192, Japan

Received October 8, 2009. Revised Manuscript Received January 15, 2010

A simple and versatile strategy has been employed to fabricate a "microreactor" consisting of nanoparticles encapsulated in a hollow core of monodispersed mesoporous silica shell. First, based on our synthesis method for monodispersed silica spheres with radially aligned mesopores, hollow mesoporous silica spheres have been synthesized using amino modified polystyrene beads as a template. We then found that introduction of metal oxide precursor into the mesoporous silica spheres using the incipient wetness technique leads to selective formation of nanoparticles into the core of the hollow spheres. Using this strategy, inorganic nanoparticles (TiO_2 and Fe_2O_3) are confined into the hollow cores, with high loading and high dispersion, to which widely accessible mesoporous channels were connected. The loading contents of TiO_2 and Fe_2O_3 were 40.2 and 36.4 wt %, respectively. These values were considered quite high when compared to values previously reported for similar materials. The photocatalytic activity of TiO_2 encapsulated silica capsules in the degradation of methyl orange was examined. The decomposition rate, especially at the initial reaction stage, for this capsule was considerably faster than that for other mesoporous silica-based TiO_2/SiO_2 composites. The methodology described here is versatile and convenient and thus can be extended to a broad range of guest species for high-performance catalysis, adsorption, and energy conversion materials.

1. Introduction

The development of nanoscience and technology has drawn significant attention to studies on hollow particles (also referred to as capsules).[1−6] Among these materials, hollow mesoporous capsules are promising because of their distinct characteristics including the large void volume and tunable porous shells. The void volume can be used for encapsulation of various guests and the porous shells provide fast transport for reaction medium with size selectivity.[7−10] Further, they function to effectively protect the encapsulated particles in the core from the surrounding environment. Therefore, a number of potential applications as "microreactors" exist in the fields of chemistry, biotechnology, and materials science.[11−13] To date, a variety of chemical and physicochemical approaches have been employed to fabricate hollow capsules with various types of shells. For example, oxides, carbon, zeolites, and polymers have been reported.[14−17] Mesoporous silica capsules are thought to be a particularly attractive structure because of the high surface area, tunable pore size, low toxicity, and mechanical and thermal stability.[18−22]

Template-assisted replication of diverse spherical particles, such as polymer latex particles, emulsions, and vesicles, have been employed to fabricate hollow mesoporous silica spheres. Rankin et al. succeeded to obtain hollow silica particles with hexagonally ordered mesopores via the

*Corresponding author. E-mail: e4610@mosk.tytlabs.co.jp.

(1) Lou, X. W.; Archer, L. A.; Yang, Z. C. *Adv. Mater.* **2008**, *20*, 3987.
(2) Caruso, F.; Caruso, A.; Mohwald, H. *Science* **1998**, *282*, 1111.
(3) Harada, T.; Ikeda, S.; Ng, Y. H.; Sakata, T.; Mori, H.; Torimoto, T.; Matsumura, M. *Adv. Funct. Mater.* **2008**, *18*(15), 2190.
(4) Kim, S.-W.; Kim, M.; Lee, W. Y.; Hyeon, T. *J. Am. Chem. Soc.* **2002**, *124*, 7642.
(5) Lu, Y.; McLellan, J.; Xia, Y. *Langmuir* **2004**, *20*, 3464.
(6) Arnal, P. M.; Weidenthaler, C.; Schuth, F. *Chem. Mater.* **2006**, *18*, 2733.
(7) Wang, Y.; Price, A. D.; Caruso, F. *J. Mater. Chem.* **2009**, *19*, 6451.
(8) Liu, J.; Liu, F.; Gao, K.; Wu, J. S.; Xue, D. F. *J. Mater. Chem.* **2009**, *19*, 6073.
(9) Li, Y. S.; Shi, J. L.; Hua, Z. L.; Chen, H. R.; Ruan, M. L.; Yan, D. S. *Nano Lett.* **2003**, *3*, 609.
(10) Li, W. J.; Coppen, M. O. *Chem. Mater.* **2005**, *17*, 2241.
(11) Chen, J. F.; Ding, H. M.; Wang, J. X.; Shao, L. *Biomaterials* **2004**, *25*, 723.
(12) Fuertes, A. B.; Sevilla, M.; Valdes-Solis, T.; Tartaj, P. *Chem. Mater.* **2007**, *19*, 5418.
(13) Ng, Y. H.; Ikeda, S.; Harada, T.; Morita, Y.; Matsumura, M. *Chem. Commun.* **2008**, *27*, 3181.
(14) Ren, N.; Dong, A. G.; Cai, W. B.; Zhang, Y. H.; Yang, W. L.; Huo, S. J.; Chen, Y.; Xie, S. H.; Gao, Z.; Tang, Y. *J. Mater. Chem.* **2004**, *14*, 3548.
(15) Zhang, L.; Qiao, S. Z.; Jin, Y. G.; Chen, Z. G.; Gu, H. C.; Lu, G. Q. *Adv. Mater.* **2008**, *20*, 805.
(16) Kanthasamy, T.; Barquist, K.; Larsen, S. C. *Microporous Mesoporous Mater.* **2008**, *113*, 554.
(17) Wang, J.; Xia, Y.; Wang, W.; Mokaya, R.; Poliakoff, M. *Chem. Commun.* **2005**, 210.
(18) Zhang, Q.; Zhang, T. R.; Ge, J. P.; Yin, Y. D. *Nano Lett.* **2008**, *8*, 2867.
(19) Feng, Z. G.; Li, Y. S.; Niu, D. C.; Li, L.; Zhao, W. R.; Chen, H. R.; Li, L.; Gao, J. H.; Ruan, M. L.; Shi, J. L. *Chem. Commun.* **2008**, 2629.
(20) Xie, B. Q.; Shi, H. F.; Liu, G. M.; Zhou, Y.; Wang, Y.; Zhao, Y.; Wang, D. J. *Chem. Mater.* **2008**, *20*, 3099.
(21) Zhao, Y.; Wang, H.; Liu, Y.; Ye, J.; Shen, S. *Mater. Lett.* **2008**, *62*, 4254.
(22) Yoon, S. B.; Kim, J. Y.; Kim, J. H.; Park, S. G.; Kim, J. Y.; Lee, C. W.; Yu, J.-S. *Curr. Appl. Phys.* **2006**, *6*, 1059.

Published on Web 01/29/2010

templating method using polystyrene microspheres under basic conditions.[23] TEM observation indicated that the cylindrical pores ran parallel to the hollow cores and individual silica particles were, in most cases, attached to the surface of the hollow particles.

Emulsion templating methods have also been investigated because they do not require removal of the core template. Fujiwara et al. have adopted the synthesis of an interfacial reaction using a water/oil/water (W/O/W) emulsion system.[24] Although they have succeeded in synthesizing mesoporous materials, the regularity of the pores was compromised and the alignment of the pores was unclear.

Mesoporous silica capsules themselves are attractive; however, the encapsulation of guest species into capsules has increased the range of potential applications because of the unique structure with a porous outside shell and functional inner core. Furthermore, the mesopores aligned perpendicular to the hollow cores are much more suitable for encapsulating the guest species and providing a fast diffusion path to the cores. There have been some reports that describe encapsulation of nanoparticles into hollow spaces. However, in most examples, either only a few nanoparticles were encapsulated or the aggregates were embedded.[25−27] Although diverse functional nanoparticles have been successfully confined within the hollow mesoporous shell in these works, the characteristics have not been investigated or somewhat insufficient properties have been shown. Therefore, fabrication of mesoporous silica capsules with a considerable amount of nanoparticles encapsulated in the hollow cores remains a challenge. To bring out the properties effectively inherent in a guest species and impart the hollow capsules with diverse capabilities, we must address the following: (a) a considerable amount of guest molecules must be encapsulated and distributed homogeneously within the hollow cores, (b) guest species must be confined only in the hollow cores and a large proportion of the porosity in the silica shell must be preserved, (c) radially aligned mesopores are preferable to guarantee easy transportation for the reaction media, and (d) uniform particle size is desirable to be achieved for practical applications or quantitative analysis.

Titanium(IV) oxide (TiO_2) has been widely studied due to its strong oxidizing ability, biological and chemical inertness, and suitability for environmental applications.[28−32] The strong oxidation ability is a great advantage of TiO_2; however, too strong oxidizing ability may also be a drawback for constructing reaction system based on TiO_2. The substrate that supports the TiO_2 as well as toxic organic pollutants may decompose via the photooxidation pathway on TiO_2. In an effort to address this problem, various methods have been reported involving the encapsulation or coating of TiO_2.[33−35] Therefore, incorporation of TiO_2 nanoparticles inside mesoporous silica capsules is expected to be a useful and attractive approach.

Herein, we present the fabrication of monodispersed hollow mesoporous silica capsules with novel and anomalous architectures. The interiors of the capsules are decorated with a large number of TiO_2 nanoparticles connected via widely accessible mesoporous channels. Amino-modified polystyrene beads were used as templates for subsequent mesoporous silica shell deposition. The synthetic condition for the mesoporous silica shell has been referred to that of the monodispersed mesoporous silica spheres (abbreviated as "MMSS" hereafter) that we previously reported.[36,37] The recipe for MMSS has important advantages over that for other mesoporous silica because radially ordered hexagonal mesopores with spherical morphology and high monodispersity can be achieved simultaneously, which helps us to reach our goal; fabricating an ideal "microreactor" that can satisfy the conditions described above. The encapsulation process described in this paper is versatile and convenient that can be extendable to a broad range of guest species. In the last part of this article, we have also demonstrated the results for Fe_2O_3 encapsulation briefly.

2. Experimental Section

Materials. All starting materials were used as received. Monodispersed amino-modified polystyrene (amino-PS) beads (200 nm diameter) were obtained as an aqueous suspension (2.5 wt %) from Polysciences (Warrington, PA). Tetramethoxysilane (TMOS), cetyltrimethylammonium chloride (CTMACl), titanium(IV) isopropoxide, acetylacetone, and potassium tert-butoxide were purchased from Tokyo Kasei Co (Japan). One molar sodium hydroxide solution, methanol, ferrocenecarbaldehyde, furfuryl alcohol, ethylene glycol, acetone, tetrahydrofuran, methyl orange, and methylene blue were purchased from Wako Pure Chemical Co (Japan). Tetra-*tert*-butyl orthotitanate was purchased from Sigma−Aldrich (USA).

Synthesis of Hollow Mesoporous Silica capsules (HMS). Monodispersed hollow mesoporous silica capsules (HMS) have been prepared from TMOS and CTMACl using amino-PS as a template and employing the synthetic procedure described for MMSS.[36] The amino group on the PS surface enables TMOS to be hydrolyzed and condensed on the PS surface without additional alkaline reagents, thus preventing independent nucleation of silica particles. Typically, at room temperature, 0.352 g of

(23) Tan, B.; Rankin, S. E. *Langmuir* **2005**, *21*, 8180.
(24) Fujiwara, M.; Shiokawa, K.; Tanaka, Y.; Nakahara, Y. *Chem. Mater.* **2004**, *16*, 5420.
(25) Kim, J. Y.; Yoon, S. B.; Yu, J.-S. *Chem. Commun.* **2003**, 790.
(26) Li, G.; Kang, E. T.; Neoh, K. G.; Yang, X. *Langmuir* **2009**, *25*, 4361.
(27) Li, L.; Ding, J.; Xue, J. *Chem. Mater.* **2009**, *21*, 3629.
(28) Choi, H.; Stathatos, E.; Dionysiou, D. D. *Appl. Catal., B* **2006**, *63*, 60.
(29) Song, W. H.; Jun, Y. K.; Han, Y.; Hong, S. H. *Biomaterials* **2004**, *25*, 3341.
(30) Schuler, M.; Trentin, D.; Textor, M.; Tosatti, S. G. P. *Nanomedicine* **2006**, *1*, 449.
(31) Sekulic, J.; Ten, Elshof, J, E.; Blank, D, H, A. *J. Sol−Gel Sci. Technol.* **2004**, *31*, 201.
(32) Xu, Y. M.; Langford, C. H. *J. Phys. Chem. B* **1997**, *101*, 3115.
(33) Ikeda, S.; Kowata, Y.; Ikeue, K.; Matsumura, M.; Ohtani, B. *Appl. Catal., A* **2004**, *265*, 69.
(34) Inumaru, K.; Kasahara, T.; Yasui, M.; Yamanaka, S. *Chem. Commun.* **2005**, 2131.
(35) Shanmugam, S.; Gabashvili, A.; Jacob, D. S.; Yu, J. C.; Gedanken, A. *Chem. Mater.* **2006**, *18*, 2275.
(36) Yano, K.; Fukushima, Y. *J. Mater. Chem.* **2004**, *14*, 1579.
(37) Nakamura, T.; Mizutani, M.; Nozaki, H.; Suzuki, N.; Yano, K. *J. Phys. Chem. C* **2007**, *111*, 1093.

CTMACl was dissolved in 80 g of methanol−water (50: 50 w/w) and 2.84 mL of the suspension of amino-PS beads and 5.28 g of TMOS were added sequentially. The reaction was allowed to proceed for 8 h under continuous stirring and the mixture was aged overnight. The particles were filtered off, washed with distilled water three times, and dried at 318 K for 72 h followed by calcination at 823 K in air for 6 h to remove the CTMACl and the PS-template.

Confinement of Inorganic Oxide Nanoparticles within the Interior Surface of HMS. In order to encapsulate the TiO_2 nanoparticles, 2.84 g of titanium isopropoxide was first mixed with 2 g of acetylacetone. This solution was added dropwise into HMS hosts until incipient wetness was achieved and subsequently heated in air at 773 K for 6 h, with supplying water vapor to the furnace. This process was repeated once or twice in order to introduce TiO_2 nanoparticles. The resultant products are designated HMS-Ti (x), where x indicates repeating number of the procedure described above (x = 1 or 2). Currently about 46.3% of TiO_2 was incorporated in HMS-Ti (2). In an effort to confine Fe_2O_3 nanoparticles in the hollow core, 2.14 g (0.01 mol) of ferrocenecarbaldehyde was first dissolved in 1 mL of furfuryl alcohol. This solution was then added dropwise until incipient wetness was reached, followed by polymerization and calcination in air at 773 K.[38] The obtained powder was denoted as HMS-Fe.

Characterization. Powder X-ray diffraction (XRD) measurements were performed using a Rigaku RINT-2200 X-ray diffractometer for the hollow mesoporous silica capsule and a Rigaku RINT-TTR X-ray diffractometer for inorganic oxide nanoparticle confined samples, using Cu Kα radiation. The morphology and the elemental composition of the powders were examined using a scanning electron microscope (SEM) equipped with an energy-dispersive X-ray (EDX) detector (Hitachi, S-3600N). SIGMA-V (Akashi Seisakusho) was also used to obtain SEMs. The sample was placed on a copper plate and the surface of each sample was coated with gold prior to measurement. The average diameter of the particles was calculated from the SEM images. Transmission electron micrographs were obtained using a JEOL-200CX TEM with an acceleration voltage of 200 kV. The particle size of the encapsulated nanoparticles was estimated from TEM images. ultrahigh resolution scanning electron microscope S-4800 (Hitachi) was also used to obtain SE and STEM images at 30 kV. Nitrogen adsorption isotherms were measured using a Quantachrome Autosorb-1 at 77 K. The specific surface areas were deduced from the analysis of the isotherm by the BET method ranging from $P/P_0 = 0.05$ to $P/P_0 = 0.15$. The pore size distributions were calculated from adsorption branches by the BJH method.

Photocatalytic Activity. The photocatalytic activity of the HMS-Ti (2) was evaluated for the decomposition of methyl orange and metylene blue under UV light irradiation. Two types of photocatalysts constructed from mesoporous silica spheres and the titanium phase were synthesized as controls. The first was monodispersed mesoporous silica spheres (MMSS) impregnated with titania nanoparticles (denoted as MS-Ti_{nano}) and the other consisted of a combination of the monodispersed titania core and the mesoporous silica shell (denoted as MS-Ti_{core}). Briefly, MS-Ti_{nano} was synthesized by incipient wetness technique using titania precursor and MMSS. In the case of MS-Ti_{core}, monodispersed spherical colloids of titania were immersed in silica precursor solution which was referred to that of MMSS. Upon calcination at 773K, mesopores in the silica shell were given rise to. Details of the synthetic conditions are described in the Supporting Information. The commercial photocatalyst Degussa P25 was also used as a reference for photocatalytic activity.

The photocatalytic activity for decomposition of methyl orange was evaluated as follows. The photocatalyst powders (25 mg) were dispersed in a 0.2 mM of methyl orange solution (10 mL) using a magnetic stirrer. After the adsorption equilibrium was reached (30 min), UV light (100 W) was supplied to initiate the reaction. A certain amount of solution was periodically taken from the reaction mixture and the supernatants were analyzed using a UV−vis spectrophotometer (Shimadzu UV-3600 UV−vis-NIR spectrophotometer) after centrifugation. The degradation ratio was calculated according to the absorbance peak at 460 nm in the spectra. To ensure a negligible heating effect upon the degradation of methyl orange, a blank experiment was conducted. A 0.2 mM of methyl orange solution without photocatalyst was irradiated with UV light and the reaction was monitored in the same manner described above. No significant decomposition of methyl orange was observed in the absence of photocatalyst under similar irradiation conditions.

To demonstrate the stability of the TiO_2 nanoparticles within HMS-Ti (2) during the photodecomposition reaction, we reused the used HMS-Ti (2) for testing another photocatalytic activity. The HMS-Ti (2) was recovered after it was tested for the decomposition of methyl orange, followed by calcination in air at 773 K to remove the residual reactant and reactivate the adsorption and catalytic properties. The obtained HMS-Ti (2) (15 mg) was dispersed in a 0.05 mM of methylene blue aqueous solution (8 mL) and shaken for 2 h in the dark to establish an adsorption equilibrium. The powder was collected by centrifugation and redispersed in water using a magnetic stirrer. UV light (100 W) was irradiated to the dispersion to evaluate the photocatalytic activity for the degradation of methylene blue.

3. Results and discussion

Fabrication of Hollow Mesoporous Silica Capsules (HMS). Figure 1 shows a schematic for the fabrication of HMS and nanoparticle-decorated HMS. The first step involves coassembly of TMOS and CTMACl by hydrophobic interactions on the PS template. In the synthesis of MMSS, sodium hydroxide is added to promote the hydrolysis and condensation of TMOS, resulting in the formation of mesoporous silica. Instead of sodium hydroxide, amino group on the PS surface plays a role as a catalyst for hydrolysis of TMOS in this procedure. Therefore, the reaction of TMOS can be restricted to only the surface of the PS beads, and no nucleation of silica particles occurs in the reaction solution. When the nonfunctionalized PS beads were used as seed particles, under otherwise identical conditions except for adding sodium hydroxide, mesoporous silica particles not linked to the PS beads were also observed. The amino-modified PS beads are thought to be a key to the fabrication of hollow mesoporous silica capsules. After removal of the PS core and CTMACl by calcination, monodispersed hollow mesoporous silica capsules were obtained. TEM and STEM images of HMS are presented in Figure 2. The TEM image of Figure 2a clearly shows the hollow silica

(38) Nakamura, T.; Yamada, Y.; Yano, K. *J. Mater. Chem. C* **2006**, *16*, 2417.

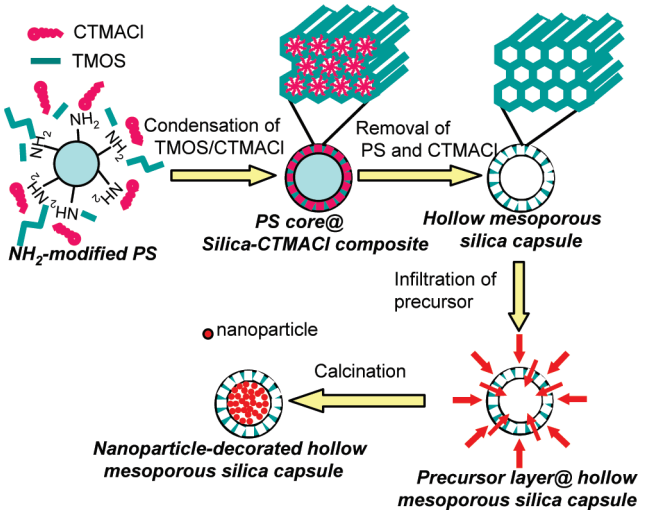

Figure 1. Schematic illustration for the fabrication of nanoparticle-decorated mesoporous silica capsule.

spheres with high monodispersity in size. The diameter of the hollow core was about 200 nm, which was consistent with the average diameter of the PS template. The thickness of the silica shell was uniform and estimated to be 30 nm, containing 2D hexagonal mesopores, as shown in Figure 2b.

The surface and mesostructure of HMS are clearly observed in STEM images. The SE image shown in Figure 2c demonstrates that HMS has a smooth surface without any deposits, and the thickness of the shell is uniform. The corresponding BF-STEM image (Figure 2d) clearly shows the mesoporous structure in the shell. Further, part of the mesopores is aligned radially from the center to the outside of the spherical particles. Such radially aligned mesopores are thought to be advantageous in encapsulating the reaction site into the hollow cores and guaranteeing facile entry and discharge of reactants and products through the silica shell when compared to the pores that run parallel to the cores or those without directional regularities.

The mesostructure in the silica shell was confirmed by XRD and nitrogen adsorption measurements (Figure 3). The XRD pattern of HMS (a) exhibited one definite peak indexed to (100) with a d spacing of 3.8 nm. A broad rise was also observed around 4−5 (2θ/deg), which was attributed to higher-order reflection peaks (110) and (200). This implies hexagonally close-packed cylindrical pores. The silica shell was thin and curved, resulting in small diffraction domains; therefore, higher-order reflections were not clearly observed. The nitrogen adsorption isotherm was type IV, which is typical for mesoporous materials. The isotherm shows a steep increase around $P/P_0 = 0.2$, indicating that the pore size distribution is quite narrow. The pore diameter calculated from the nitrogen adsorption isotherm was 20 Å by the BJH method and the specific surface area was 1040 $m^2\ g^{-1}$. It should be noted that the BJH method, which is used in this study for estimating the pore size, is not the most suitable approach for the evaluation of small mesopores like our materials. DFT or some careful estimation[39] might be recommended to obtain more accurate values. However, because the BJH method has been widely applied in many reports,[40,41] including the references of this study,[21,25] the BJH method has been chosen to evaluate the pore size.

Decoration of Hollow Mesoporous Silica Capsules with TiO_2 Nanoparticles (HMS-Ti). SEM images and the corresponding EDX spectra are shown in Figure 4. The HMS samples were found to maintain their monodispersity and spherical morphology after the titanium infiltration process. The EDX signal at 1.74 keV, assigned to silicon, was observed for both HMS-Ti (1) and HMS-Ti (2). These results provide conclusive evidence that the shell of the hollow capsule consisted of SiO_2. In HMS-Ti (x), the signal attributed to titanium is observed at 4.5 keV and the signal intensity increases with number of the repeated infiltration cycles. The copper signal was attributed to the copper plate that the sample was fixed on for observation. The amount of loaded TiO_2 was estimated from EDX analysis and is listed in Table 1.

The amount of encapsulated TiO_2 in the hollow mesoporous capsule is 13.7 wt % for the HMS-Ti (1) and increased drastically to 40.2 wt % for the HMS-Ti (2). It is important to note that in spite of such a high loading of TiO_2, the SEM images show no extra TiO_2 particles on the surface of HMS-Ti (x). TEM images of HMS-Ti (2) are shown in Figure 5. These images demonstrate the unique structure of the prepared samples. The TiO_2 nanoparticles, observable as black dots, were almost entirely encapsulated in the hollow core and very few were deposited in the mesopores of the silica shell. This was verified by the inset of Figure 5b, which shows an enlarged image of the boundary between the mesoporous silica shell and the hollow core of HMS-Ti (2). The boundary between the silica shell and the hollow core is a sharp black line where the TiO_2 nanoparticles are concentrated. In addition, the TiO_2 (uniform size of 8.3 nm obtained from the TEM image) is well-dispersed in the inner surface of the shell. A selected area electron diffraction (SAED) pattern obtained for the HMS-Ti (2) (Figure 5c) confirms that the encapsulated TiO_2 nanoparticles are the anatase phase.

The crystal structure of the encapsulated TiO_2 was analyzed by XRD measurement (Figure 6a). For HMS-Ti (1), the diffraction intensity was not strong, but for HMS-Ti (2) with high TiO_2 loading, a pattern with a strong intensity was observed and can be indexed as the anatase phase, which is consistent with the crystal structure obtained from the SAED pattern. The size of the crystals was estimated to be 8 nm, by applying Scherer's equation to the main peak of the XRD pattern. This finding is in good agreement with that obtained from the TEM images (8.3 nm).

Nitrogen adsorption measurements for HMS-Ti (x) were conducted and the results are shown in Table 1

(39) Kruk, M.; Jaroniec, M. *Chem. Mater.* **2001**, *13*, 3169.

(40) Kobler, J.; Möller, K.; Bein, T. *ACS Nano* **2008**, *2*, 791.
(41) Chi, Y.-S.; Lin, H.-P.; Mou, C.-Y. *Appl. Catal., A* **2005**, *284*, 199.

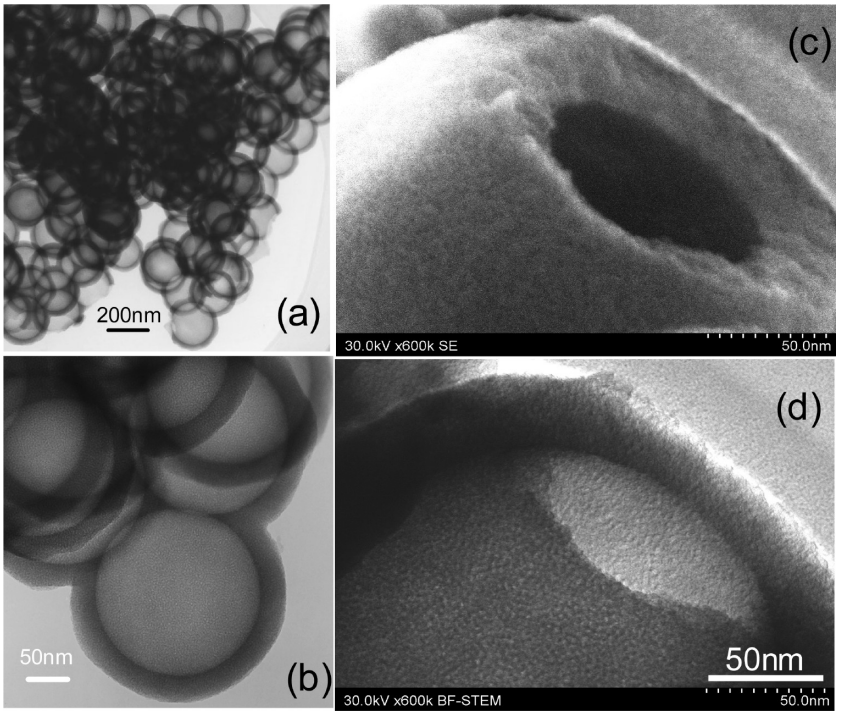

Figure 2. TEM images of HMS at (a) low and (b) high magnifications. (c) Secondary electron (SE) and (d) corresponding bright-field scanning transmission electron microscopy (BF-STEM) images for a single HMS particle.

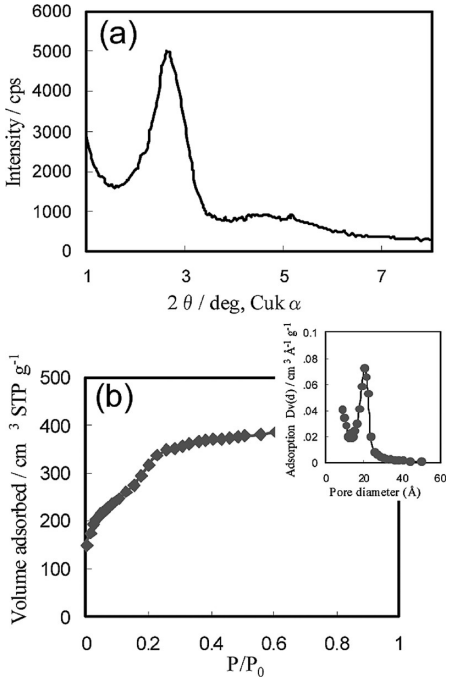

Figure 3. (a) XRD pattern and (b) nitrogen adsorption isotherm for HMS. The inset in (b) shows corresponding pore size distribution curve.

and Figure 6 b. (Nitrogen adsorption isotherms are shown in the Supporting Information, Figure S1).

The BET surface area and pore volume decreased with increasing the infiltration cycle. However, the pore diameter was fairly constant. Further, the BET surface areas expressed on a SiO_2 mass basis (normalized to SiO_2 content) were 988 and 893 m^2/g for HMS-Ti (1) and HMS-Ti (2), respectively. In the case of HMS-Ti (2), the reduction in the BET surface area was very small

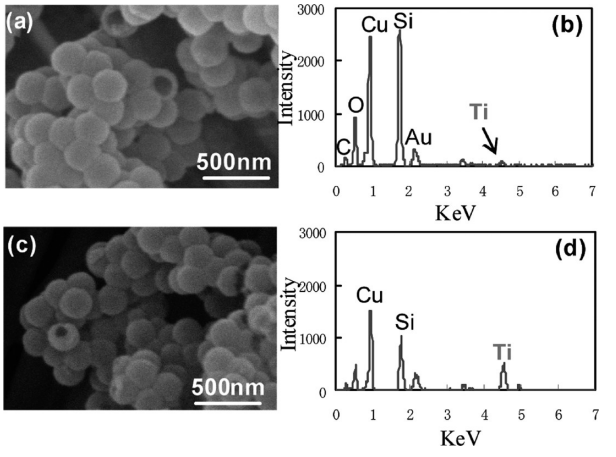

Figure 4. (a, c) SEM images and (b, d) energy-dispersive X-ray spectra for (a, b) HMS-Ti (1) and (c, d) HMS-Ti (2).

Table 1. Structural Properties for Samples

	TiO_2 loading wt %[a]	specific surface area (m^2g^{-1})[b]	specific surface area/m^2g^{-1}[c]	pore diameter/nm
HMS	/	1040	←	2.0
HMS-Ti(1)	13.7	853	988	2.0
HMS-Ti(2)	40.2	534	893	1.9
MMSS	/	1394	←	2.2
MS-Ti_{nano}	12.7	1090	1250	1.9
MS-Ti_{core}	82.2			

[a] Content of TiO_2 in the samples estimated by EDX. [b] BET surface area expressed on a sample mass basis. [c] BET surface area expressed on a SiO_2 mass basis.

regardless of the large TiO_2 content (40 w%) in the capsules, retaining almost 86% of the initial value. The result indicates that most of the TiO_2 was encapsulated in the large hollow core, and hardly deposited in the

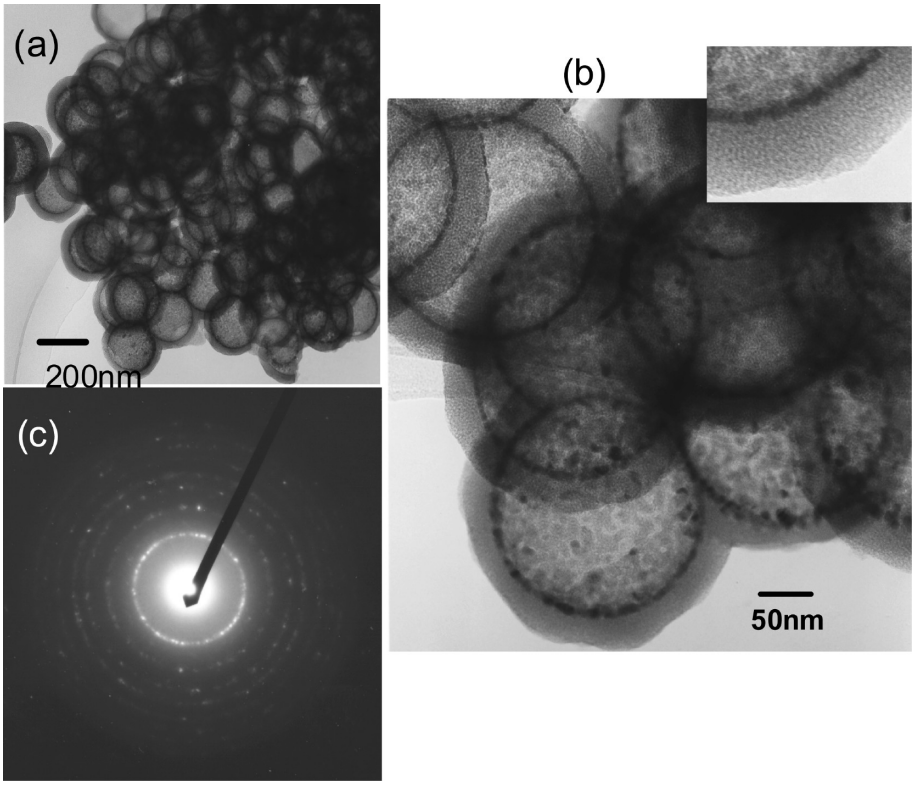

Figure 5. TEM images of MHS-Ti (2) at (a) low and (b) high magnifications. The inset of (b) is an enlarged view of the interior surface of HMS-Ti (2) showing titania nanoparticles confined within the interior surface of the hollow spheres. (c) Selected-area electron diffraction (SAED) pattern for the encapsulated titania nanoparticles.

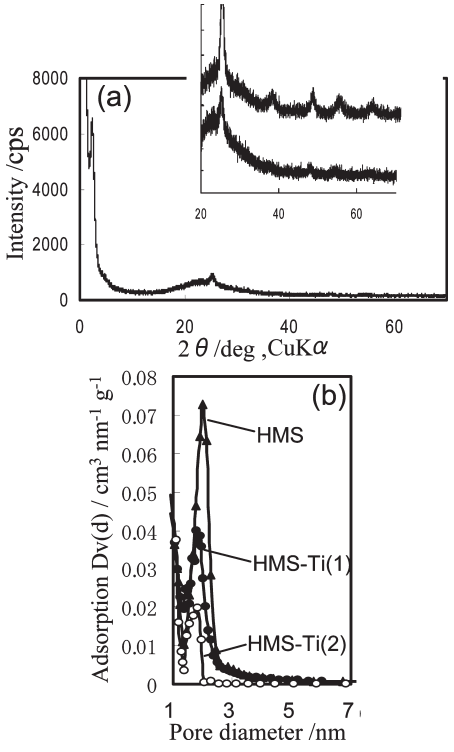

Figure 6. (a) XRD patterns for HMS-Ti (1). Inset: Enlarged view of wide-angle XRD patterns for HMS-Ti (1) (lower) and HMS-Ti (2) (upper). (b) Pore size distribution for HMS (▲), HMS-Ti (1) (●), and HMS-Ti (2) (○).

mesopores of the silica shell. This assumption is in good agreement with the result obtained from TEM observation.

The mechanism of formation of HMS-Ti (interior surface was selectively decorated with a large amount of TiO_2 nanoparticles) is as follows. In the case of HMS with the mesopores connected to the hollow core, the precursor solution is introduced into the mesopores of the silica shell by capillary force, which induces differences in the concentration of precursor solution between the hollow core and the mesopores. Such a concentration difference provides the driving force to accelerate the diffusion of precursor solution from the mesochannel to the inner core. Once the inorganic precursor is introduced into the hollow cores, they prefer to aggregate rather than to be isolated in mesopores in order to reduce the surface energy. The aggregates of the precursor that are larger than the mesopores are prevented from being retracted into the mesochannels and are converted into inorganic nanoparticles by successive heat treatment. The volume of the hollow core is so large compared to that of a mesochannel, therefore, the concentration difference of the inorganic precursor between outside and inside of the core can not be eliminated. Thus, the driving force behind filling the hollow core with the inorganic precursor is strong enough to bring a large amount of nanoparticles into the core without depositing the precursor in the mesochannel. In this way, hollow mesoporous silica capsules with inner surfaces decorated with a large amount of inorganic nanoparticles are obtained.

The preservation of mesoporous channels is important for applications that require facile entry and discharge of reactants and products through the mesoporous silica

shell. One appropriate example in which such a system would be of use is when encapsulated nanoparticles are adapted as catalysts. As is mentioned in Introduction, a number of mesoporous silica capsules have been proposed and some have functional reaction sites introduced into them. However, among these, HMS-Ti is the best candidate for use as a "microreactor" composed of confined catalytic sites connected with widely accessible mesoporous channels which offer rapid transportation. We can point out a possibility to use HMS-Ti as novel high-performance catalysts by modifying them on the basis of our knowledge. We have succeeded in synthesizing various types of core/shell MMSS.[42,43] One of them has consisted of a catalytic active site (sulfonic acid) in the core and an adsorption site (hydrophobic organic groups) in the shell.[43] The resulting core/shell type MMSS has shown higher catalytic activities than MMSS having randomly distributed SO_3H and hydrophobic groups. The composition of the core/shell structure can be tuned freely; therefore, by confining TiO_2 nanoparticles within the inner core of the core/shell structures, which are designed for the catalytic reactions, new types of selective catalysts or multistep reaction catalysts can be realized. It is believed that such particles consisting of tailor-made type multilayers will be advantageous for both fundamental and applied research.

Preparation of Reference Samples and Comparison with HMS-Ti. The unique characteristics of HMS-Ti can be confirmed by comparing it to MS-Ti_{nano}, which is composed of MMSS (mesoporous solid silica spheres) impregnated with TiO_2 nanoparticles. Characterization of MS-Ti_{nano} was conducted and the results are summarized in the Supporting Information (Figure S2). The SEM image (Figure S2a in the Supporting Information) shows that hardly any deposits are observed on the surface of MMSS, and the monodispersed spherical shape was retained after TiO_2 infiltration. The EDX (Figure S2b in the Supporting Information) spectrum and a wide-angle XRD pattern (Figure S2c in the Supporting Information) have confirmed the immobilization of anatase TiO_2 within MMSS. However, the ratio of Si/Ti estimated by EDX was 84.3/15.7, which corresponded to ca. 12.7 wt % TiO_2 loading. This value was significantly lower than that obtained for HMS-Ti (2) (40.2 wt %). The amount of nitrogen adsorbed as well as the pore diameter for MS-Ti_{nano} has decreased to 1.9 nm from the initial value (2.2 nm) obtained for MMSS. The BET surface area normalized to the SiO_2 content is 1250 $m^2\ g^{-1}$ for MS-Ti_{nano}, retaining 89.6% of that of MMSS (1390 $m^2\ g^{-1}$). Results indicate that unlike HMS-Ti (2), only a small amount of TiO_2 nanoparticle loading causes a noticeable decrease in the pore diameter and the BET surface area for MS-Ti_{nano}. These decreases are associated with the pore-filling effect[44] because of the incorporation of the TiO_2 nanoparticles into the mesopores of the solid materials.

In addition, it is important to increase the amount of encapsulated TiO_2 nanoparticles in the practical use. However, previous attempts to increase the impregnated TiO_2 nanoparticles in the MMSS were unsuccessful. In order to increase the amount of TiO_2 in the MS-Ti_{nano}, infiltration of the titania precursor was in triplicate. In most cases, aggregates were observed on the surface of MMSS (see the Supporting Information Figure S3). It was clearly shown that encapsulation of a substantial amount of nanoparticles into the solid porous materials, into which the concentration difference of precursor solution was small, was quite difficult.

We have succeeded in synthesizing another photocatalysts (MS-Ti_{core}) having a unique architecture composed of titania core[45] and mesoporous silica shell. The SEM images show that the monodispersity and the spherical shape of titania spheres are well-inherited after the addition of a silica source (Figure S4a,c in the Supporting Information). The average particle sizes are 390 and 400 nm for titania spheres and MS-Ti_{core}, respectively, indicating that the titania core is coated with a thin layer of silica. The generation of a silica shell is also confirmed using an EDX spectrum that shows a definite signal assigned to silicon (Figure S4d in the Supporting Information). The ratio of Si/Ti was estimated to be 14.4/85.6. The XRD pattern reveals that the crystal structure of titania particles is anatase (Figure S4e in the Supporting Information). The nitrogen adsorption−desorption isotherm for MS-Ti_{core} was measured to investigate the porosity of the silica shell (Figure S4f in the Supporting Information). Although the amount of adsorbed nitrogen is relatively low, the isotherm can be classified as type IV, with a capillary condensation step, which is characteristic of mesoporous materials. To confirm the alignment of the mesopores, we performed TEM observation on the core/shell particles (Figure S5 in the Supporting Information). The synthetic conditions were slightly altered in order to promote the growth of the silica shell for more facile observation.

The TEM image of the obtained particles (Figure S5a in the Supporting Information) clearly shows an egg-type structure, indicating it is composed of a titania core and silica shell. Radial alignment of ordered mesopores in the silica shell is substantiated by the enlarged view shown in Figure S5b in the Supporting Information. This result suggests that the shell of HMS may also be composed of radially aligned mesopores, because the synthesis of mesoporous silica shells is almost identical for HMS and MS-Ti_{core}.

Photocatalytic Activity. To explore potential applications of HMS-Ti (2) as a "microreactor" for catalysis, we carried out UV-induced photocatalytic decomposition of methyl orange (MO). As controls, the catalytic activities of MS-Ti_{core} and MS-Ti_{nano} were also examined. MO was selected as a reactant because the amount of MO

(42) Yano, K.; Nakamura, T. *Chem. Lett*. **2006**, *35*, 1014.
(43) Suzuki, T. M.; Nakamura, T.; Sudo, E.; Akimoto, Y.; Yano, K. *J. Catal*. **2008**, *258*, 265.
(44) Gierszal, K. P.; Yoon, S. B.; Yu, J. S.; Jaroniec, M. *J. Mater. Chem. C* **2006**, *16*, 2819.
(45) Jiang, X. C.; Herricks, T.; Xia, Y. N. *Adv. Mater*. **2003**, *15*, 1205.

adsorbed into mesoporous silica is negligible. In combination of mesoporous silica and active titania, one can expect mesoporous silica of high adsorption performance, because of large specific surface areas, prior to photodecomposition on the surface of titania. However, whether adsorption or photodecomposition contributes to the reduction of the reactant can not be distinguished because these two functions occur simultaneously.[46]

Additionally, the point we mention the most in this study is that HMS can provide easy entry and discharge of reactants and products from the outer environment to the inner core where activation sites are encapsulated. Vice versa, by adopting MO as a reactant in this study, structural advantage of the HMS-Ti, which provides the fast diffusion path through the mesopores, can be precisely evaluated.

Figure 7 shows the results of the photocatalytic degradation of MO under UV light as function of irradiation time with schematic illustration for fabricated photocatalysts. One of the advantages of the HMS-Ti (2) is the high capacity of TiO_2 within the structure. The residual ratio is calculated based on the sample weight (Figure 7a), which is important in describing the feature of the HMS-Ti (2). HMS-Ti (2) showed high photocatalytic activity compared to the controls. The absorbance of MO as function of irradiation time significantly decreased, especially at the initial stage, and the residual ratio reached nearly 10% in 2.5 h. On the other hand, the MS-Ti_{core} and the MS-Ti_{nano} exhibited the values of 60 and 85%, respectively, in 2.5 h. The photocatalytic activity was evaluated based on the residual ratio; the performance of the HMS-Ti (2) was about 2.2 times as high as that of MS-Ti_{core}, and about 5.8 times as high as that of MS-Ti_{nano}. The superiority of HMS-Ti (2) concerning the catalytic activity was maintained, even when the decomposition of MO was expressed on a TiO_2 mass basis (Figure 7b).

The lowest decomposition rate of MO was observed for MS-Ti_{core}. This was attributed to large titania diameter[47,48] (390 nm) in spite of accompanying the active anatase structure with the accessible mesochannels.

The particle sizes of TiO_2 for MS-Ti_{nano} are estimated to be below 2 nm because they are encapsulated within the mesopores of MMSS (2.2 nm), the value is smaller than that obtained for HMS-Ti (2). Judging from the impregnated TiO_2 particle size, the photocatalytic activity of MS-Ti_{nano} is supposed to be equivalent, or rather superior, to HMS-Ti (2). The diffraction peak intensity of anatase titania is lower for MS-Ti_{nano} than that observed for HMS-Ti (2); however, the crystallinity of these two catalysts are expected to be comparative because the impregnation of titania precursor and the crystallization condition are the same. It is implied that the difference observed for the XRD diffraction patterns are due to the size and the amount of TiO_2 particles. The catalytic

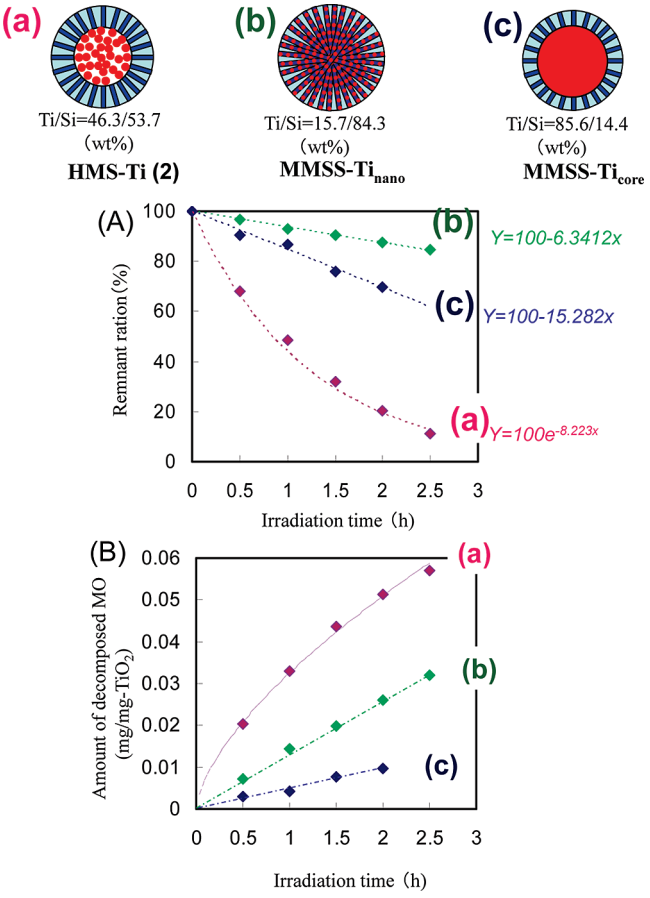

Figure 7. Photocatalytic degradation of methyl orange under UV light as function of irradiation time. Mesoporous silica capsules confining titania nanoparticles (HMS-Ti(2), pink), mesoporous silica spheres impregnating titania nanoparticles (MS-Ti_{nano}, blue), and titania core mesoporous silica shell spheres (MS-Ti_{core}, green). Approximate expressions are also shown on the right side. (B) Result expressed on a TiO_2 mass base.

activity shown in Figure 7 suggests that HMS-Ti (2) is superior to MS-Ti_{nano}. It is to be noted that the inherent properties (e.g., crystallinity, crystal sizes) of the TiO_2 particles often play definitive roles in the catalytic activity. We can not determine the contributing ratio of such inherent properties precisely, due to the lack of the absolute value of the TiO_2 particle sizes for MS-Ti_{nano}. However, on the basis of the discussion above, the enhanced catalytic activity of HMS-Ti (2) shown in Figure 7b is assumed to be derived from the structural specificity of the HMS-Ti (2). That is, in the case of HMS-Ti (2) the reaction sites with high catalytic activity were well-dispersed over the internal capsule walls into which reaction medium was carried through radially aligned mesopores, supplying a fast diffusion path. The fast diffusion path of the mesopores within HMS-Ti (2) are suggested by the shape of the MO decomposition curve. MO decomposition was approximated by a linear first-order reaction for the MS-Ti_{core}, and MS-Ti_{nano}. On the other hand, HMS-Ti (2) displayed an exponential decay curve in which the MO decomposition rate was especially high in the initial reaction stage. The obtained result strongly supports the idea that the anomalous shape of HMS-Ti (2) is advantageous for the photocatalytic reaction because of the fast diffusion path.

(46) Li, J. J.; Liu, S. Q.; He, Y. Y.; Wang, J. Q. *Microporous Mesoporous Mater.* **2008**, *115*, 416.
(47) Maira, A. J.; Yeung, K. L.; Lee, C. Y.; Yue, P. L.; Chan, C. K. *J. Catal.* **2000**, *192*, 185.
(48) Liu, S.; Jaffrezic, N.; Guillard, C. *Appl. Surf. Sci.* **2008**, *255*, 2704.

In the case of P25, the amount of decomposed MO reached 0.026 mg, based on the titania weight, in 0.5 h and the MO dispersion turned clear within 1 h. This result indicates that the catalytic activity of the commercial photocatalyst P25 is higher than that of HMS-Ti (2). As is described in the Introduction, there have been many reports about encapsulation or coating of TiO_2 particles with various kinds of substrates to provide selective photocatalytic functions. However, this approach seems to incur an unavoidable result that it decreases intrinsic photocatalytic activity of the TiO_2 particles because of the surface coverage over them. Another possible reason for the lower catalytic activity of HMS-Ti (2) is aggregation of the particles, as are observed in SEM or TEM images, caused by the small particle size. It is well-known that the dispersity of catalyst is very important in solution-phase catalysis. And it is also known that small particles tend to aggregate. In this study, we used amino-PS beads with diameter of 200 nm as sacrificial scaffolds and it was difficult to obtain a well-dispersed suspension from them during the condensation of silica source. Choosing PS template with a larger diameter will lead to the improvement of the dispersibility, thus photocatalytic activity for the resultant HMS-Ti.

Next, to demonstrate the advantage of HMS-Ti (2) over P25 as well as the stability of the encapsulated TiO_2, another catalytic reaction involving adsorption process, which takes advantage of the mesopores in the shell, was conducted (see the Supporting Information, Figure S6). As was clearly observed in Figure S6 a, the adsorption of methylene blue to the mesopores of HMS-Ti (2) is thought to proceed efficiently because the particles were colored blue after centrifugation. The commercial photocatalyst P25 remained white after the same adsorption procedure due to the lack of adsorption ability. The methylene blue adsorbed on HMS-Ti (2) decomposed rapidly under UV irradiation. The obtained result strongly indicates the advantage of HMS-Ti (2) derived from its unique structure, which provides adsorption ability as well as photocatalytic activity for realizing highly selective photocatalytic functions. It should be noted that adsorption and degradation of methylene blue were evaluated using the recovered HMS-Ti (2) after the photodecomposition reaction of MO. The photocatalytic efficiency as well as the adsorption property was maintained, suggesting that the stability of the TiO_2 nanoparticles on the inner wall of the HMS capsule and the mesostructure in the capsule is high enough for recycling.

Herein, we have focused on mesoporous silica capsules encapsulating TiO_2 nanoparticles, however, nanoparticles are not only restricted to TiO_2. To demonstrate the versatility of this system, we have also decorated the interior surface of mesoporous silica capsules with Fe_2O_3 nanoparticles (denoted as MHS-Fe) and the results are shown in the Supporting Information (Figure S7). The content of Fe_2O_3 in the hollow mesoporous capsule was estimated to be 36.4 wt % from EDX analysis, which is considerably high for a single infiltration. Previously, we reported fabrication of Fe_2O_3/MMSS composite spheres obtained from the same infiltration process.[38] The loading content of Fe_2O_3 in the composite attained 19 wt %, which was quite high compared to other reported mesoporous silica-based Fe_2O_3/SiO_2 composites. However, the number obtained for the MHS-Fe, 36.4 wt %, was much higher than that of the Fe_2O_3/MMSS composite spheres. In spite of such a high loading of Fe_2O_3, no extra particles were observed on the surface of Fe_2O_3 loading capsules, as is clear from the SEM image (see Figure S7b in the Supporting Information). Decoration of the interior surface of hollow mesoporous silica capsules with Fe_2O_3 nanoparticles was confirmed by the TEM image (see Figure S7a in the Supporting Information). Application of the MHS-Fe as a drug delivery vehicle is currently underway in our laboratory. This procedure can be readily extended to other functional nanoparticles. Further studies to produce an ideal microreactor by changing the variety and quantity of the nanoparticles are also under investigation.

4. Conclusions

In summary, we have succeeded to fabricate uniform hollow mesoporous silica capsules (HMS) and to decorate the interior surface of the cores with highly dispersed inorganic oxide nanoparticles.

Taking advantage of the synthesis method for monodispersed silica spheres with radially aligned mesopores, HMS have been synthesized using amino-modified polystyrene beads as a template. Incipient wetness technique has been found to bring about selective formation of a large amount of nanoparticles into the cores of the HMS. Although TiO_2 and Fe_2O_3 nanoparticles were successfully encapsulated in the hollow cores of HMS, the mesopores of the silica shell contained very few nanoparticles. The loading contents of TiO_2 and Fe_2O_3 were high, 40.2 and 36.4 wt %, respectively. Photocatalytic activity of TiO_2 encapsulated HMS was investigated and the systems displayed high performance in the degradation of methyl orange, especially at the initial stage of the reaction. The obtained results were thought to be blessed with the anomalous architecture, which is composed of a large amount of confined active catalysts connected with widely accessible mesoporous channels. The methodology reported herein is versatile and convenient and can be extended to a broad range of guest species, which can be easily incorporated in mesoporous materials. Taking advantage of such a unique architecture, these composites are expected to be used in a wide range of applications as a novel "microreactors" such as high-performance catalysis and energy conversion materials.

Acknowledgment. The authors are grateful to Noritomo Suzuki (TEM images) and Hiroaki Kadoura (STEM images).

Supporting Information Available: Nitrogen adsorption isotherms, characterization and synthetic condition of the MS-Ti_{nano}, characterization and synthetic condition of the MS-Ti_{core}, adsorption and decomposition of methylene blue, and characterization of HMS-Fe (PDF). This material is available free of charge via the Internet at http://pubs.acs.org.